Role of Aromatic Crosslinks in Structure and Dynamics of Model Three-stranded β-Sheet Peptides

David Scheerer,[1] Heng Chi,[2,3] Dan McElheny,[2] Ayesha Samer,[2]

Timothy A. Keiderling,[2]* Karin Hauser[1]*

[1] Department of Chemistry, University of Konstanz, 78457 Konstanz, Germany

[2] Department of Chemistry, University of Illinois at Chicago, Chicago, IL, USA,

[3] Jiangsu Food and Pharmaceutical Science College, Huai'an, China,

Abstract

A series of closely related peptide sequences that form triple-strand structures were designed with a variation of cross-strand aromatic interactions and spectroscopically studied as models for β-sheet formation and stabilities. Structures of the three-strand models were determined with NMR methods and temperature-dependent equilibrium studies carried out using CD and FTIR spectroscopies. Our equilibrium data show that the presence of a direct cross-strand aromatic contact in an otherwise folded peptide does not automatically result in an increased thermal stability, and can even distort the structure. The effect on the conformational dynamics were studied with infrared detected temperature-jump relaxation methods and revealed a high sensitivity to the presence and the location of the aromatic crosslinks. Aromatic contacts in the three-stranded peptides slow down the dynamics in a site-specific manner and the impact seems to be related to the distance from the turn. Using a Xxx-^{D}Pro linkage as a probe with some sensitivity for the turn, small differences were revealed in the relative relaxation of the sheet strands and turn regions. In addition, we analyzed the component hairpins which showed less uniform dynamics as compared to the parent three-stranded β-sheet peptides.

INTRODUCTION

β-sheets are essential elements of protein secondary structure and have become a prime focus for study of initial steps in protein misfolding. Experimental study of sheets is impaired by their non-sequential character in which strand segments must come together to form sheets in a manner that can be independent of their sequence in a larger molecule (polypeptide). If single, separate strands interact in this way, the result is an oligomer of indeterminate size, which can even grow (sometimes irreversibly) to become a larger aggregate or fibril.[1-2] Folding studies of peptide models then must be able to discriminate intermolecular from intramolecular cross-strand H-bonds leading to β-sheet formation. One approach used in many labs has been to design and study hairpins where a single strand folds back on itself to create two antiparallel segments that are cross-strand H-bonded with a turn or loop between them.[3-4] These hairpins can then be studied as monomeric species, but each strand has intramolecular H-bonds on only one side, being solvated on the other. In practice such structures are also highly twisted and the ends tend to fray.[5-6] Designing a sequence with added turns and thus more β-strands thereby creating a multi-strand sheet model is the natural extension of the hairpin approach. In such a design the inner segments can be fully cross-strand H-bonded, assuming minimal distortion at the turns or loops and the termini. Several examples of such structures exist in the literature.[7-11]

Analysis of β-sheet formation is best done with infrared (IR) methods,[11-15] since electronic circular dichroism (ECD) yields very weak bands in the near UV for sheet structures. By contrast, ECD has been used to monitor changes in the interactions of aromatic side chains, particularly for the Trpzip series of molecules that were initially designed by Cochran and co-workers.[16-20] Such an aromatic interaction is essentially

a tertiary effect that is at some level independent of the cross-strand H-bonding of the sheet secondary structure. Using ECD to monitor temperature variation of structures with interacting aromatic residues can yield insight into the stabilizing effects of hydrophobic interactions distinct from structure formation associated with backbone H-bonds. IR of the amide C=O stretch (amide I band) is sensitive to the H-bonding, but even more to the coupling of these amide modes both in the strand (through-bond) and cross-strand (through-space). Following the IR absorbance changes with variation in temperature permits determination of stability and equilibria of folded and unfolded β-sheet like conformers, assuming simple behavior. In contrast to the ECD, the IR changes are independent of and resolved from the spectral effects of aromatic coupling. Dynamics of the folding and unfolding processes can be followed using IR methods, but peptide folding processes are quite fast (sub microsecond),[21-23] so that conventional mixing or denaturant dilution experiments are inadequate. To address this, laser-induced temperature-jump (T-jump) relaxation kinetics methods are employed here to access these faster rates.

In this study, three related triple-strand model peptides were designed and synthesized along with their constituent (two-stranded) hairpins. The peptide folds were stabilized by use of ^{D}Pro-Gly residues to initiate the turns but the sequences varied in the location of cross-strand hydrophobic interaction by Trp-Tyr aromatic residues. Modeling the folding is enhanced by determination of the folded structure for the target three-stranded peptides by NMR methods. Stabilities of the β-sheet structures were studied with equilibrium temperature-dependent CD and IR. The focus of this report is the comparison of their β-strand dynamics as determined with amide I´ IR-detected T-jump relaxation kinetics.

METHODS

The peptides used in this study are modelled after the sequence design principles developed by Gellman and coworkers for their ^{D}Pro-Gly stabilized hairpins,[7,24] with additional stabilization by cross-strand Trp-Tyr interactions following designs of Cochran and Waters.[16,20] Three different three-stranded β-sheet peptides were prepared (see Table 1): **1W-2Y-3L** has a Trp-Tyr interaction between strand 1 (Trp) and 2 (Tyr) with a Leu on strand 3, while **1L-2Y-3W** interchanges the Leu und Trp residues to give an aromatic interaction between strands 2 (Tyr) and 3 (Trp). As a control, **1I-2Y-3L** has an alternate design with essentially the same sequence but with the aromatic residues, in this case Phe and Tyr, now on opposite sides of the designed sheet. Naturally this requires the exchange of an added residue to eliminate the cross-strand stabilizing interaction but still retains the ^{D}Pro-Gly turns as the main structure-forming element and maintains the relative hydrophobicity of the three-stranded structure. For comparison, a series of two-stranded β-hairpins were prepared, which have sequences identical to either the strands 1-2 or 2-3 of the corresponding three-stranded peptides. These are used to investigate the relative influence of the first or third strand on the equilibria and dynamics of the other two.

Table 1: Sequences of the studied three-stranded and two-stranded peptides.

Type	Peptide[a]	Sequence[b]			Side Chain Variation
		strand 1- turn 1	strand 2	turn 2 - strand 3	
three-stranded	**1W-2Y-3L**	SVKI**W**TS-pG	KT**Y**TEV	pG-TKT**L**QE-NH_2	aromatic contact strand 1-2
	1L-2Y-3W	SVKI**L**TS-pG	KT**Y**TEV	pG-TKT**W**QE-NH_2	aromatic contact strand 2-3
	1I-2Y-3L	SVKF**I**TS-pG	KT**Y**TEV	pG-TKT**L**QE-NH_2	no aromatic contact
two-stranded[c]	**1W-2Y**	SVKI**W**TS-pG	KT**Y**TEV-NH_2		strand 1-2 of 1W-2Y-3L
	2Y-3L		KT**Y**TEV	pG-TKT**L**QE-NH_2	strand 2-3 of 1W-2Y-3L/1I-2Y-3L
	1L-2Y	SVKI**L**TS-pG	KT**Y**TEV-NH_2		strand 1-2 of 1L-2Y-3W
	2Y-3W		KT**Y**TEV	pG-TKT**W**QE-NH_2	strand 2-3 of 1L-2Y-3W
	1I-2Y	SVKF**I**TS-pG	KT**Y**TEV-NH_2		strand 1-2 of 1I-2Y-3L

[a] Nomenclature used emphasizes the strand on which the interacting/exchanged hydrophobic group is located

[b] Strand 2 is the same for all variants, the amino acids interchanged in the strands 1 and 3 are underlined; residues responsible for the nomenclature are marked bold

[c] The 2-stranded peptides are the constituent hairpins of the three-stranded ones

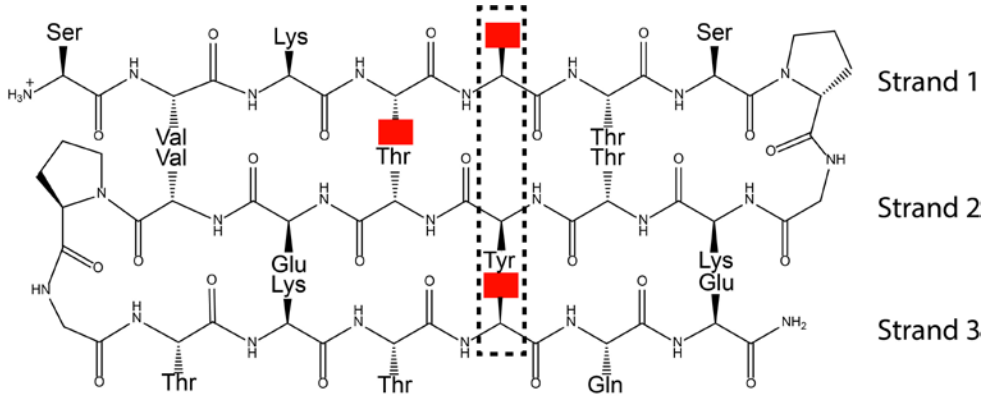

Scheme 1: Generic layout of the three-stranded sheet model. Red boxes indicate residues interchanged, dashed black frame shows the location of possible aromatic crosslinks. Positions 5 and 21 are Trp and Leu for **1W-2Y-3L** and vice versa for **1L-2Y-3W**. To place the aromatics on opposite sides, so there can be no interaction, three changes are needed, where positions 4, 5 and 21 are Phe, Ile and Leu, respectively, for **1I-2Y-3L**. The component hairpins make up either the N-terminal strands 1 and 2 or the C-terminal strands 2 and 3 of the corresponding three-stranded β-sheet.

Peptide synthesis and purification. Peptides were obtained from SciLight Biotechnology LLC, Beijing, China, after being synthesized using standard FMOC methods, cleaved from the resin, purified with HPLC (95-99% purity) and

characterized with MALDI mass spectroscopy. For IR studies, to eliminate spectral interference from trifluoroacetate (TFA) counterions remaining from the peptide preparation, peptides were dissolved in 0.1 M DCl and lyophilized three times. Then the peptides were redissolved in D_2O at concentrations of ~10 mg/mL.

NMR structure determination. Peptides were dissolved in 90:10, H_2O:D_2O, at about 6 mg/mL concentration (~2-3 mM). 1-D ^{1}H-NMR and 2-D COSY spectra were obtained on a Bruker 500 MHz instrument, and NOESY and TOCSY spectra were obtained with a Bruker Avance 800 MHz instrument, all at 283 K, with gradient selection and excitation sculpting for water suppression.[25] 2-D NOESY were acquired (mixing times = 80 and 300 ms) with 12 ppm sweep widths, 2048x1024 complex points in t_2 x t_1 and 16 scans per increment. 2-D TOCSY were acquired under similar conditions with DIPSI2 mixing of 70 ms and a radio-frequency field of 8 kHz. All spectra were processed within NMRPipe[26] and viewed/assigned in NMRView.[27] Data regarding spectra accumulation and results used for the structure determinations are available in Table S1 of the Supporting Information (SI). The NOESY peaks were manually selected and assigned with CYANA 2.0.[28] The lowest energy structures were selected from an ensemble of 100 and further refined by restrained MD following a previously described methodology within AMBER8,[29] using the ff99sb force field.[30] The resulting 10 unique structures with the lowest AMBER and restraint violation energies were subjected to structure validation within PROCHECK_NMR.[31]

Equilibrium CD, fluorescence and IR. Samples for CD study were prepared at ~0.2-0.3 mg/mL in phosphate buffer (H_2O) at pH 7.5 and were measured in a 1 mm path quartz cell on a JASCO 815 spectrometer using 1 s time constant, 1 nm bandwidth and averaging 8-12 scans (spectra were corrected using UV-absorbance

to determine actual concentrations, which ranged from 0.1 to 0.6 mM). Temperature was fixed by a JASCO Peltier sample holder operated under instrument control, and varied from 5 to 85 ^{o}C in steps of 5 ^{o}C. Fluorescence of the same samples was measured on a Horiba Fluoromax 4, also with a Peltier sample temperature control accessory. Spectra were measured every 5 ^{o}C from 5 to 80 ^{o}C by scanning emission from 300 to 500 nm with excitation at 270 nm.

IR and VCD samples were prepared in D_2O at ~10 mg/mL at acidic pH (after lyophilization from DCl) and were placed in homemade demountable cells consisting of CaF_2 windows separated by a Teflon spacer with 100 µm optical pathlength. IR and VCD spectra for the same samples were acquired on a Bruker Vertex 80 FTIR with a DTGS detector and on a homemade dispersive VCD spectrometer[32] (in Chicago) or on a Bruker Equinox 55 FTIR spectrometer equipped with a mercury cadmium telluride (MCT) detector (in Konstanz). IR measurements in both labs were in agreement, and only IR spectra done in Konstanz, on the same samples as used for the T-jump experiments, are further discussed here. The room temperature VCD confirmed formation of β-sheet conformation in the three-stranded constructs, but for this dynamics oriented study did not add to the analyses and will not be discussed further. For each FTIR spectrum, 128 scans with a spectral resolution of 4 cm^{-1} were averaged at each temperature. Thermal variation of the IR spectra was carried out in the temperature range of 5–95 °C in steps of ΔT = 5 °C. The temperature of the sample holder was controlled by a water bath (Lauda Ecoline E300, Germany), with the sample cell temperature recorded by a Pt100 sensor. A home-built software-controlled shuttle device was used to measure the sample and reference signal successively for each temperature allowing the subtraction of the solvent signal.

Temperature variations of the CD and IR data were typically quite gradual, with no characteristics of a sharp transition. Several methods of analyses were attempted, and the best fits in terms of scatter of the data points, statistical quality of fit, and reproducibility of repeated measurements on separate samples were obtained by use of singular value decomposition (SVD).[33] SVD naturally segregates the noise to higher components and utilizes changes in the entire bandshape being considered. The second component represents the major variance from the average (or first component), and its loading is typically the most sensitive to the change being studied, particularly for amide I' IR spectra where the absorbance is roughly constant and the differences are relatively small bandshape and frequency shifts. The fits were made to a sigmoidal equation with flat baselines (for details see SI) to obtain just the transition temperature, T_m, (inflection point) since the data sets did not have enough curvature to fit more variables (e.g. sloped baselines or ΔH). Parameters describing such gradual transitions might be sensitive to singular poor data points, so this was tested using the Jack Knife error analysis in the fitting program GLOVE,[34] whereby the data set with one data point successively left out was fit, and the process was repeated dropping the next point and continuing through the entire set. The standard error of this set of fits provides a measure of quality of fit and sensitivity to data point deviations. Further details on analyses of multiple sample data sets are in the SI.

Temperature-jump dynamics measurements. T-jump data were obtained on similarly prepared samples as used for IR thermal studies. Some samples showing small absorbance changes were rerun at higher concentration without qualitative changes in the kinetics. T-jump measurements were performed using the quantum cascade laser-based (QCL) spectrometer that has been described in detail previously.[35-36] Briefly, the T-jump excitation is provided by a Q-switched Ho:YAG

laser (IPG Photonics Corporation, U.S.A.) operated at 2090 nm. The Ho:YAG laser pulses excite a D_2O overtone vibration leading to a rapid increase in temperature within the excited volume. For a 10 Hz repetition rate the pulse duration is 9 ns and the maximum pulse energy 14 mJ. A chopper was synchronized with the pump laser to block alternate pulses, which allows acquisition of reference signals under identical conditions, but with no pump light at the sample, and results in an excitation repetition rate of 5 Hz. The pump pulse is split by a 50:50 beam splitter into two counter-propagating beams to provide more homogenous heating. The spot size of the excitation beam is about 2 mm in diameter. In order to adjust the magnitude of the T-jump, different neutral density attenuators were used to reduce the excitation energy. For most samples, a T-jump of $\Delta T \sim 8$ °C was used, but a smaller jump was needed to obtain the lowest final temperatures of about 5 °C.

To monitor the relaxation dynamics, the single wavelength emission of the QCL (Daylight Solutions Inc., U.S.A.), with a tunable range between 1715 cm^{-1} and 1580 cm^{-1}, was used as a cw probe source. The QCL beam was focused to a diameter of ~ 300 µm at the center of the excited volume. A photovoltaic MCT detector (18 MHz, KMPV11−1-J2, Kolmar Technologies, U.S.A.) was used to detect the transient changes in the probe beam transmission. The signals were digitized and recorded by a transient recorder board with 16 bit resolution (Spectrum, Germany).

The initial sample temperature was controlled by a water bath connected to the sample holder. The final temperature (after the jump) was calculated by referencing the derived absorbance change of the solvent at the respective wavelength to the corresponding temperature-dependent FTIR spectra of D_2O.[35] Usually around 2000 transients were averaged to reduce noise. To exclude distorted transients caused by cavitation effects,[37] a self-developed software filter (MATLAB2010, The MathWorks,

U.S.A.) was applied to save the most reliable data after collection. To account for solvent kinetics, both solvent and peptide sample were measured sequentially. The solvent-only signal was scaled appropriately and subtracted from the peptide sample signal.

The resulting transients were subjected to a quasi-logarithmic averaging procedure so that an equal number of points were distributed in each time decade (20 points per decade) leading to a significant reduction of noise and distortion signals. The relaxation kinetics were evaluated in a time interval from 300 ns up to 1.2 ms using a mono-exponential decay function for the three-stranded peptides as well as for the hairpins **2Y-3L** and **2Y-3W** (strands 2-3 of the three-stranded peptides). The relaxation dynamics of the hairpins which constitute the strands 1-2 of the three-stranded peptides (i.e. **1W-2Y**, **1L-2Y** and **1I-2Y**) were fit best by a bi-exponential decay function. The relaxation time constants were determined for different final temperatures varying from 7 to 60 °C and fit to an Arrhenius-like relation $k = A \exp\left(-\frac{E_a}{RT}\right)$ to represent relative thermal dependences. The measured transients, and thus the derived relaxation rates, have a reproducibility error which can be estimated from repeated measurements. For transients with large absorbance changes, the error is about $\pm$ 150 ns. However, for the lowest final temperatures (<10 °C), where absorbance changes were often relatively small, the error was larger.

RESULTS

The peptides were designed to fold into a three-stranded sheet and to allow interaction of Trp-Tyr aromatic residues on neighboring strands (for **1W-2Y-3L** or **1L-**

2Y-3W), in comparison to virtually the same sequence but without direct cross-strand interaction of aromatic side-chains (for **1I-2Y-3L**). This design succeeded, in that all three peptides were reasonably soluble (up to > 20 mg/mL), showed CD spectra reflecting a Trp-Tyr interaction where expected (**1W-2Y-3L** and **1L-2Y-3W**), gave amide I´ IR patterns characteristic of β-structures, had dispersed NMR bands and evidenced unfolding upon heating. The constituent two-stranded hairpins derived from these structures gave notably less well-formed sheets, as evidenced by their spectral patterns and less dispersed NMR, and were less stable. The comparison of the three-stranded β-sheets dynamics is the core of this report, but first we give a brief summary of their NMR structures and equilibrium behavior, which assists our interpretation of the dynamics.

NMR structures. Each of the three-strand models gave resolved NOESY and TOCSY spectra with reasonable dispersion that could be fully assigned and from which the structures could be evaluated. The **1W-2Y-3L** (aromatic contact strand 1-2) and **1I-2Y-3L** (no aromatic contact) variants formed more complete β-sheet folds than the **1L-2Y-3W** (aromatic contact strand 2-3), and this structural difference is reflected in all the spectral results that follow. None-the-less all three peptides had structures showing the essential elements of a three-stranded anti-parallel sheet with two β-turns as can be seen in Fig. 1, where the 10 best structures of each sequence are overlapped (on the left) and compared to the best structure (based on the fit to NMR parameters) for each presented with more atomic detail and the aromatic residues highlighted in red (on the right). The numbers of NOE and other structural parameters used as described above in the Methods section are enumerated for each structure in Table S1 of the Supporting Information (SI). The **1I-2Y-3L** had significantly more assignable NOEs than the other two, including 50 more long-range

NOEs. The derived structures had very similar deviations from ideal bond lengths and angles and low RMS deviations from the mean structures, but the **1I-2Y-3L** ensemble of structures again showed lower deviations from the mean than the other two, with **1L-2Y-3W** being significantly worse, as is clearly evident in Fig. 1b.

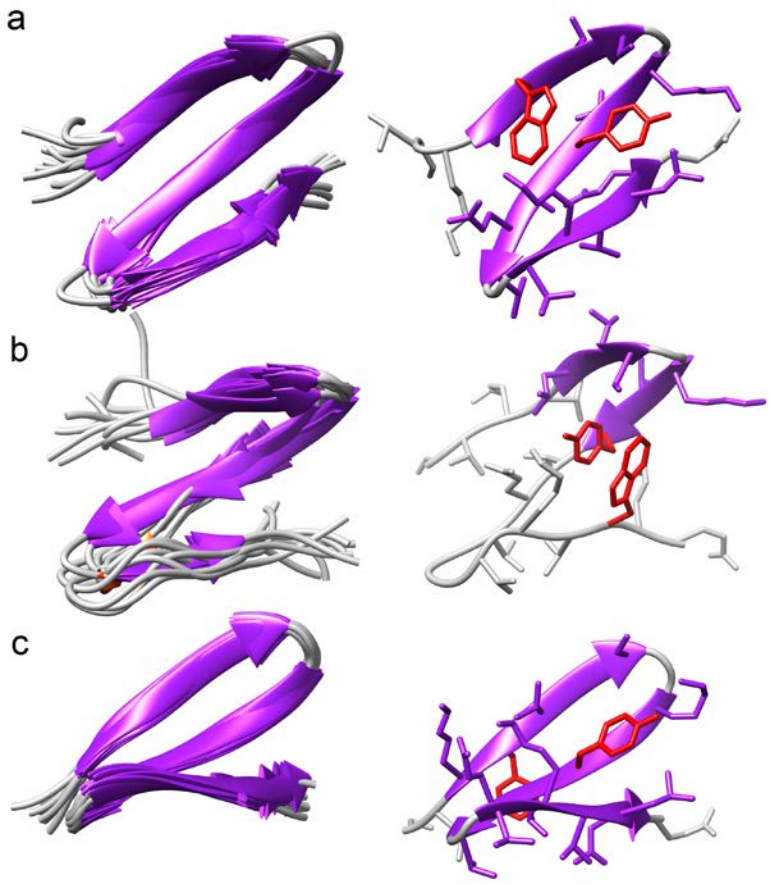

Figure 1: NMR structures of the 3-stranded β-sheet peptides. a) **1W-2Y-3L** (aromatic contact strand 1-2); b) **1L-2Y-3W** (aromatic contact strand 2-3); c) **1I-2Y-3L** (no aromatic contact). 10 solution structures are overlayed in the left column and the best fit representative structure is shown in the right column, together with the aromatic side-chains highlighted in red.

In each peptide the strands 1-2 formed a better hairpin than did strands 2-3, with the C-terminus tending to be more disordered than the N-terminus. To form each hairpin, the ^{D}Pro-Gly turns had dominantly type I' character,[38] however the ensemble of structures contained some examples in a type II' form. The variation in turn type occurred more often for the second turn, between strands 2-3, closer to the C-

terminus, and was more evident for the **1L-2Y-3W** than for the **1W-2Y-3L** or **1I-2Y-3L** peptides. The added uniformity in terms of turns as well as strands for **1I-2Y-3L** implies that the aromatic interaction did not stabilize a single turn type in this design.

Surprisingly, with no (direct) aromatic cross-strand contacts, the **1I-2Y-3L** ensemble of the 10 best structures had the least variation in turn type and gave what appears to be the best formed β-sheet structure, in terms of extended strands and cross-strand H-bond formation. All the peptides were strongly twisted, in a right-handed sense for the strands, as often observed for β-sheets of L-amino acids. These are perhaps more twisted than seen in many globular proteins, but seem less so than most of the Trpzip hairpins we have previously studied.[17-18, 39] The N-terminal hairpin, strands 1-2, was better formed than the C-terminal one, strands 2-3, in all structures, despite the shift of the aromatic cross strand interaction to strands 2-3 for **1L-2Y-3W**.

The aromatic Trp-Tyr interaction is less well defined and uniform than we previously saw in Trpzip peptides.[17-18] It seems to be more of a stacking than edge-to-face interaction, with more offset in **1W-2Y-3L** than for **1L-2Y-3W**, as can be seen by the red colored residues in the right-hand single conformer structures in Fig. 1. The aromatic contact distances were quite stable, averaging 4.6 $\pm$ 0.2 Å for **1W-2Y-3L** and 4.4 $\pm$ 0.4 Å for **1L-2Y-3W** (for the center of the Trp to the Tyr-Cγ position). This contrast of **1L-2Y-3W** and **1W-2Y-3L** peptides along with the striking uniformity of the **1I-2Y-3L** set of structures argues that despite the addition of cross-strand aromatic interaction, the turn constraint provided by the ^{D}Pro-Gly sequences appears to be the dominant structure forming element in these sequences, but there certainly is an added impact of varying the cross-strand hydrophobic and hydrophilic interactions. Our comparative spectral studies further address that variation.

Equilibrium CD and fluorescence. The CD spectra show evidence of cross-strand Trp-Tyr coupling in the form of a strong couplet at 230 (+) and 214 (-) nm, for the **1W-2Y-3L** sequence (Fig. S2, SI). From the NMR results, the orientation of the **1W-2Y-3L** Trp-Tyr pair is somewhat between that reported for the Trpzip Tyr-Trp mutants we previously studied (more angle, edge-on-face),[18] and the overlapped stacking seen here (Fig.1) for **1L-2Y-3W**. The **1W-2Y-3L** CD reflects, but is not exactly the same as and is weaker than what we have reported for Trp-Tyr mutants of Trpzip2. Thus the overall ECD shape supports a Trp-Tyr interaction. For the **1L-2Y-3W** the interaction and resulting CD is clearly different, and makes a smaller contribution to the observed CD intensity, which is here dominated by a negative-positive couplet (or the opposite and also shifted sign pattern) at low temperature. Our previous theoretical analyses (for selected geometries only) indicated that for Trp-Trp, the intensity for stacked interactions would be less than that for edge-on-face, which might partially explain these variations for Trp-Tyr interactions.[19]

With no cross-strand aromatic contact, the **1I-2Y-3L** peptide has a negative band at ~215 nm and positive at ~200 nm, more closely reflecting that expected for a β-sheet structure. By contrast, in the other two cases, the CD cannot be straightforwardly used to determine or even give much insight into the secondary structure, but rather primarily reflects the relative coupling of the aromatic residues. At high temperatures there is still a significant negative contribution at 217 nm, as one might expect of a β-sheet, but that may be due to residual turn character caused by the conformationally restricted ^{D}Pro-Gly structure. More importantly, there is also a growth in negative contribution to the band at 200 nm, which is characteristic of increasing disorder. The temperature variation of the CD was fit using the second component of the SVD analysis for the smoothed spectra over the entire 190-250 nm region. The T_m values

for **1W-2Y-3L** and **1I-2Y-3L** were similar, with **1W-2Y-3L** (~65 °C) being always higher than for **1I-2Y-3L (**~55 °C) as summarized in Table S3, SI. By contrast, the **1L-2Y-3W** transition was quite different with a T_m of ~16 °C, which is consistent with its less well-formed β-sheet structure seen in the NMR (Fig. 1b).

The component hairpins that contain a Trp residue gave CD spectra that reflect those of the three-strand peptides from which they were abstracted. The **1W-2Y** had an intense ± couplet at ~228 and 213 nm, respectively, indicating some structure formation, patterned on that in **1W-2Y-3L**; the **2Y-3W** also had a ± couplet, weaker than for **1W-2Y** but stronger than for **1L-2Y-3W**, with a more dominant negative band at ~195 nm, implying a different aromatic contact in the hairpin or more contribution from disorder in the peptide. The non-Trp containing hairpins gave much weaker CD, with complex shapes, but the most intense bands indicated contributions from a disordered peptide conformation. Thermal transitions for the hairpins were less well defined than for the three-stranded peptides and, even based on SVD analyses, we obtained physically sensible fits for only some of them. The **1W-2Y** peptide had a high T_m with relatively low error, which is consistent with its stronger aromatic cross-strand interaction and more dispersed NMR than seen with the other hairpins. The other aromatic linked hairpin, **2Y-3W** had a much lower T_m with a similar error. Both were less sensitive to alternate methods of analysis than the non-aromatic linked hairpins.

Considering the fluorescence spectra, the peptides which contain Trp gave an emission band with a maximum at ~355 nm that dropped off sharply, and nearly linearly with increase in temperature. This is consistent with the aromatic residues being solvated and on the surface of the three-strand structure, and consequently they offer little insight into folding or stability, and will not be discussed further.

Equilibrium IR. The IR spectra of all the three-stranded variants (see Fig. S4, SI) exhibited an amide I' (indicating H-D exchange of the amide NH in D_2O) band pattern which is characteristic for β-hairpins, having a more intense peak at ~1638 cm^{-1} and a shoulder to higher wavenumbers at ~1675 cm^{-1}. Additionally, another shoulder is observed at ~1612 cm^{-1}, which can be attributed to the Xxx–^{D}Pro tertiary amides that sequentially precede the two β-turns.[40] The amide I' VCD showed a relatively weak couplet bandshape with a sharper negative at 1625 cm^{-1} and broader, weaker positive at ~1670 cm^{-1} for both **1W-2Y-3L** and **1L-2Y-3W** which is consistent with β-structure formation but offers little insight beyond the IR results and will not be analyzed further. At high temperatures the IR band broadens and shifts to ~1650 cm^{-1}. The unfolding process is very gradual with some β-sheet structure appearing to remain even at high temperatures. The transition temperatures were obtained by applying SVD to the IR temperature variation and fitting the 2nd component of the SVD with a sigmoidal function (results of which are illustrated in Fig. 2).

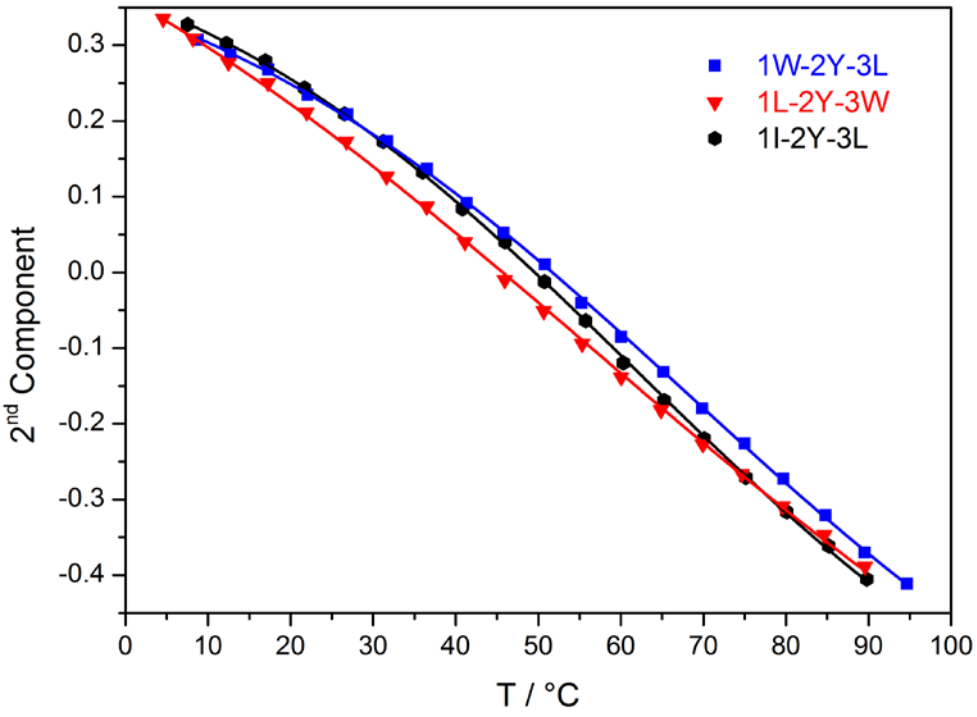

Figure 2: Differences in thermal stability between the three-stranded β-sheet models. The corresponding midpoint of the thermal transitions $\boldsymbol{T_m}$ were 68 ± 4 °C for **1W-2Y-3L** (blue), 56 ± 5 °C for **1L-2Y-3W** (red) and 62 ± 3 °C for **1I-2Y-3L** (black) as obtained for IR of the amide I´ region (1600-1700 cm^{-1}) using SVD and fitting the 2nd component the SVD with a sigmoidal equation with flat baselines. The data shown are for a selected sample run, but the T_m values are derived by global fits to multiple data sets for different samples (see Table S10, SI).

The band shape changes (essentially a frequency shift) yield transition temperatures of: T_m ~ 68 °C for **1W-2Y-3L**, T_m ~ 62 °C for **1I-2Y-3L** and a lower T_m ~ 56 °C, for **1L-2Y-3W,** based on global fits to separate sample data sets. The transition temperatures confirm that the **1L-2Y-3W,** which has the least developed β-sheet structure, is additionally the least stable (lowest T_m, as also seen with CD, but with less difference). The **1I-2Y-3L** and **1W-2Y-3L** have higher transition temperatures, with the **1W-2Y-3L** (having hydrophobic aromatic cross-strand stabilization) being the highest. The IR frequency changes reflected in the second SVD component are mostly due to loss of cross-strand coupling and H-bonds in the β-strands, which are

well developed but to different extents in all three peptides. Qualitatively the same pattern was seen with CD, which reflects the aromatic coupling where present, but the IR T_m values are generally higher than found with CD. Alternate fitting methods were attempted, including selecting intensities at characteristic frequencies and the method of Gai and co-workers, using the integrated intensity of the 1680 cm^{-1} band.[41] None of these gave as good quality of fits as found with the SVD approach reported here, which utilizes the maximal changes of the full band.

The equilibrium spectra (Fig. S5 and S6, SI) of the constituent hairpins show that the strands 1-2 form more developed β-structure than the strands 2-3, independent of having any aromatic contact. For the N-terminal hairpins the spectra resemble those of the three-stranded variants with an intense peak at ~1637 cm^{-1} and a shoulder at ~1675 cm^{-1} at low temperatures. Only for the **1L-2Y** is the β-sheet band shifted to higher wavenumbers (1640 cm^{-1}) indicating a more disordered structure. This is in good agreement with the transition temperatures and NMR structures for the three-stranded β-sheets, where the **1L-2Y-3W** does not have as extensive β-structure as the other two. For the C-terminal hairpins the β-sheet band is blue-shifted even further (~1643 cm^{-1}) and the high-frequency component is less pronounced, especially for the **2Y-3L,** which contains no aromatic interaction. This reflects the increased disorder of the C-terminal strands in the parent structures as was observed in the three-strand parent NMR results. Reinforcing these qualitative observations, the midpoint of the unfolding transition is about 20 °C lower for the C-terminal hairpins than for the N-terminal ones (see Fig. S7-S9 and Table S10, SI).

Temperature-jump dynamics. The T-jump experiments were performed at selected wavenumbers in the amide I′ region that were determined from the maximum absorbance changes in the FTIR equilibrium data. Changes in the β-sheet structure

were primarily sensed at ~1630 cm^{-1}, and the Xxx–^{D}Pro tertiary amide band at ~1612 cm^{-1} was used as a potential probe for the turn region, although it is not exclusive since it senses the turn-to-strand link. Relaxation data for all the three-stranded β-sheet peptides and constituent hairpins have been measured by IR detected T-jump kinetics. Representative transients for the β-sheet structure (1632 cm^{-1}, blue curve) and the Xxx–^{D}Pro band (1612 cm^{-1}, green curve) are shown in Fig. 3 for **1I-2Y-3L** as an example. The data, after correction for solvent dynamics, were fit well to a mono-exponential function for each of the three-stranded variants, however for some of the two-strand hairpins (N-terminal sequences) a bi-exponential function was required, as will be discussed below.

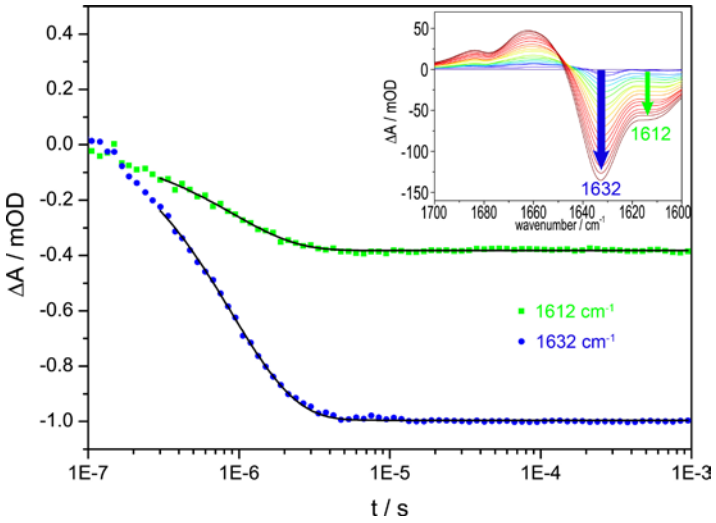

Figure 3: Transient signal after the laser-excited temperature-jump shown for **1I-2Y-3L** with a final temperature of 26.7 °C as an example. Relaxation kinetics were monitored at 1612 cm^{-1} for the Xxx-^{D}Pro turn amide (green) and at 1632 cm^{-1} for the β-sheet structure (blue). The inset shows the equilibrium FTIR difference spectra of **1I-2Y-3L** upon heating from 5°C (reference; blue) to 95 °C (red) which were used to select the probe wavenumbers for the T-Jump experiment.

All the variants have in common rigid ^{D}Pro-Gly turns which promote hairpin formation[7, 42] and inhibit total unfolding of the structure. These peptides exhibit quite fast relaxation times, less than 4 μs. Fig. 4a summarizes the relaxation times, plotted against the final temperature, for the three-stranded variants as measured at

~1630 cm^{-1}, the β-sheet band. Much as we have seen with various Tyr-substituted Trpzip2 mutants,[43] the high temperature rates (> 25°C) of the three-stranded models were very fast (τ~ 500 ns) and differences between the peptides were not resolvable. However at low peptide temperatures, there is variation, with the **1L-2Y-3W** being distinctly slower. In Table 2 values of relaxation times at two selected temperatures are compared as obtained from the best fit of all the T-jump kinetic data to an Arrhenius relationship. The **1I-2Y-3L** variant, with no aromatic interaction between the strands, shows the fastest relaxation, with, for example, τ = 1.43±0.04 μs at T_{final} = 10 °C. The **1W-2Y-3L** variant has virtually the same kinetic profile, relaxing only slightly more slowly at low temperatures (τ = 1.72±0.16 μs at 10 °C). However the **1L-2Y-3W** peptide, whose NMR structure and other spectral properties show more differences from the more completely formed sheet structures, is significantly slower (τ = 2.37±0.38 μs at 10 °C).

Table 2: Selected relaxation time constants probed at ~1630 cm^{-1} and ~1612 cm^{-1} obtained from fits to the Arrhenius relationship.

Peptide	τ [μs][a] at ~1630 cm^{-1}		τ [μs][a] at ~1612 cm^{-1}	
	10 °C	35 °C	10 °C	35 °C
1W-2Y-3L	1.72(±0.16)	0.65(±0.05)	2.17(±0.19)	0.55(±0.06)
1L-2Y-3W	2.37(±0.38)	0.49(±0.14)	2.70(±0.28)	0.60(±0.11)
1I-2Y-3L	1.43(±0.04)	0.47(±0.05)	1.65(±0.03)	0.51(±0.03)
1W-2Y	1.16(±0.12)	0.36(±0.03)	-	-
2Y-3L	0.55(±0.02)	0.10(±0.03)	0.55(±0.09)	0.11(±0.09)
1L-2Y	[4.18 (±1.00)][b]	0.26(±0.09)	-	-
2Y-3W	0.98(±0.05)	0.21(±0.04)	1.01(±0.11)	0.17(±0.06)
1I-2Y	0.84(±0.08)	0.32(±0.03)	-	-

[a] the error was determined by the regular residual as the mean of individual measurements in a temperature range of T = 7.5-12.5 °C or T = 32.5-37.5 °C

[b] low reliability and exceptionally large error due to very low absorbance changes at low temperatures

A similar pattern is observed for the temperature dependence of the Xxx–^{D}Pro dynamics measured at 1612 cm^{-1} (see Fig. 4b). At high temperatures τ again is around 500 ns, but at low temperatures the three peptides deviate in their relaxation time constants, with **1I-2Y-3L** being clearly faster than **1W-2Y-3L** and **1L-2Y-3W**, the latter of which is again slowest. However, in contrast to the 1630 cm^{-1} β-sheet band, the thermal profile of the 1612 cm^{-1} Xxx-Pro detected kinetics for **1W-2Y-3L** resembles more that of **1L-2Y-3W** than of **1I-2Y-3L**. These differences in thermal behavior of the rates for 1630 cm^{-1} and 1612 cm^{-1} do indicate some influence of the turn dynamics on the overall relaxation process.

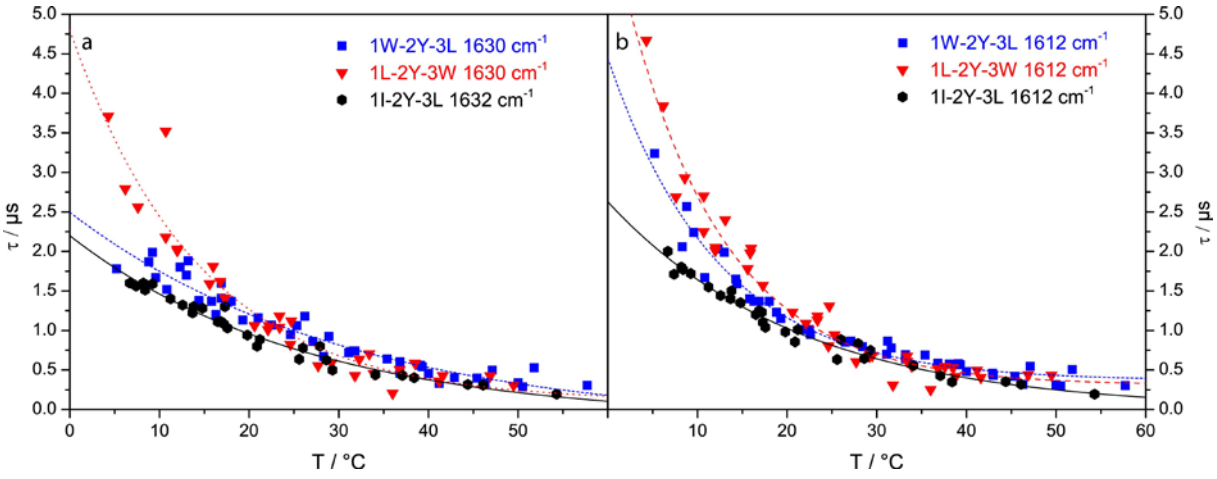

Figure 4: Relaxation times of **a)** the 1630 cm^{-1} β-sheet band and **b)** 1612 cm^{-1} Xxx–^{D}Pro band for the three-stranded β-sheet variants **1W-2Y-3L** (blue squares), **1L-2Y-3W** (red triangles) and **1I-2Y-3L** (black hexagons) in a temperature range of T_{final} = 5 - 60 °C. The lines indicate fits to the Arrhenius equation giving a qualitative description of relative temperature variation of the relaxation rates.

As compared to the equilibrium data from CD and IR, the dynamic behaviors of the constituent hairpins show different sequence variation dependencies that provide

more insight into the folding process. For the C-terminal hairpins, **2Y-3W** and **2Y-3L**, constituting strands 2-3 of the three-strand structures, the β-strand and Xxx-^{D}Pro dynamics track each other very closely with temperature change (see Fig. 5). These hairpin rates are both significantly faster than for the three-strand variants, but **2Y-3W**, containing an aromatic cross-strand interaction, is slower than **2Y-3L,** without one.

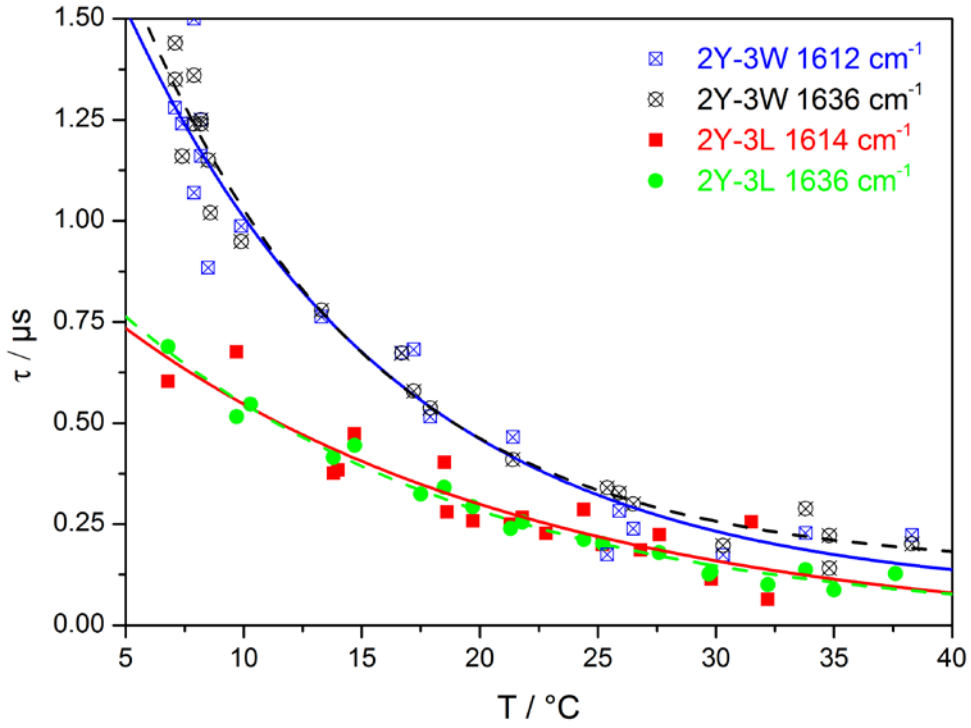

Figure 5: Relaxation times of the Xxx-^{D}Pro turn (~1612 cm^{-1}, squares, solid lines) and the β-sheet (1636 cm^{-1}, circles, dashed lines) for the C-terminal β-hairpins **2Y-3W** and **2Y-3L** in a temperature range of T_{final} = 5-40 °C. For both hairpins, the relaxation times for the β-sheet band (blue for **2Y-3W** and red for **2Y-3L**) are very similar to the Xxx-^{D}Pro band (black for **2Y-3W** and green for **2Y-3L**). The lines indicate fits to the Arrhenius equation.

However, the N-terminal hairpins, **1W-2Y**, **1L-2Y**, **1I-2Y**, had more complex behaviors, and their rates could be better determined with a bi-exponential fit (TableS11). For these, the fast components, τ_1, had values (Table 2) somewhat

faster than the relaxation rates of the three-stranded sheets (with the exception of **1L-2Y**). By contrast, the values of τ_2 were unusually slow for unimolecular β-hairpin dynamics.[13, 35, 44] We could not determine the origin of this slow component, but it may be due to the formation and population of some type of multimer. We assume that the dynamics are separable and that folding rates of the secondary structure elements are not affected by the slow process. Consequently, we here focus mainly on the fast relaxation rates for these peptides (Fig. 6) which are also summarized in Table 2.

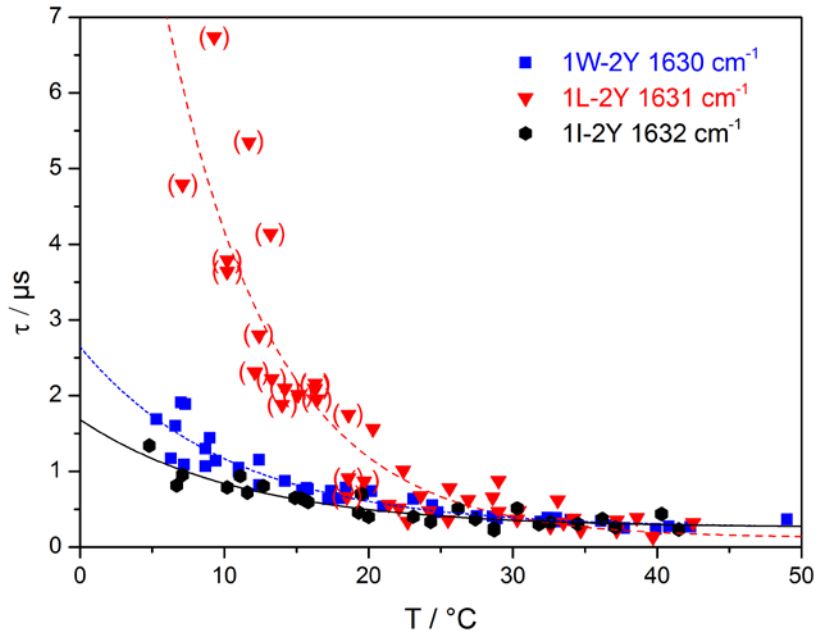

Figure 6: Relaxation times of the β-sheet band for the N-terminal β-hairpins **1W-2Y** (blue squares), **1L-2Y** (red triangles) and **1I-2Y** (black hexagons) in a temperature range of T_{final} = 5 - 50 °C. Shown are values for the fast component $\boldsymbol{\tau_1}$ of a bi-exponential fit of the respective transients. The absorbance changes of **1L-2Y** at final temperatures < 20 °C (data point in brackets) are very low, therefore these values have higher error and are less reliable. The lines indicate fits to the Arrhenius equation.

As seen in Fig. 6, the scatter in the rates for the N-terminal hairpins is much higher than for the C-terminal ones, due to their smaller change in absorbance on loss of

structure with increase in temperature, but some trends can still be seen. Relaxation of **1I-2Y** is the fastest of these N-terminal variants followed by **1W-2Y**, with **1L-2Y** being significantly slower. Since the absorbance change observed for **1L-2Y** at final temperatures below 20 °C is very low, those relaxation times are likely to be not very reliable (data points in brackets, Fig. 6). Therefore we consider **1L-2Y** as an outlier and do not evaluate this data further. Both other N-terminal hairpins, **1I-2Y** and **1W-2Y,** relax faster compared to the three-stranded variants, much as seen for the C-terminal hairpins, with the low temperature rates for **1W-2Y** being somewhat slower than for **1I-2Y**, which may be due to the **1W-2Y** aromatic contact. The Xxx–^{D}Pro band was not further evaluated for these peptides, due to its much lower absorbance changes, for which kinetics could not be reliably evaluated.

DISCUSSION

Role of aromatic contacts on thermal stability and structure. The relative thermal stabilities of the three-stranded β-sheet structures studied here can be evaluated by comparison of their different transition temperatures (Table S3 and S10, SI). All of our peptides have broad thermal transitions, and their T_m values consequently must be viewed more as qualitative indicators. To improve reliability, we analyzed the data using various fitting approaches in an effort to highlight the role of aromatic contacts on thermal stability. The equilibrium IR data reflect β-strand formation, whereas CD spectra monitor primarily cross-strand aromatic interaction, if present. The correlation between T_m values and the degree of β-strand development in the three-strand structures is more complex than we might have anticipated. While **1W-2Y-3L,** with strand 1-2 aromatic contact, has the highest T_m, it does not have the best defined

NMR structure nor the most complete β-strand formation. The **1L-2Y-3W,** with a very similar sequence, has both the lowest T_m and the worst formed structure. The **1I-2Y-3L**, with no aromatic contact, has a somewhat lower T_m than **1W-2Y-3L**, yet develops the best defined structure with most complete β-strands. Comparison of **1W-2Y-3L** and **1I-2Y-3L** suggests that the aromatic contacts of strand 1-2 result in the stability increase of **1W-2Y-3L**, but at the same time create some distortion of the β-strands. Similarly, comparison of **1L-2Y-3W** with **1W-2Y-3L**, while keeping in mind that **1I-2Y-3L** has the best developed β-strand fold, suggests the placement of the aromatic contact on strands 2-3 is both less stabilizing and leads to more distortion of the third strand.

Our design sought to create a set of peptides with very minor differences, namely the placement of aromatic residues. To minimize residue changes and keep the aromatic contact on one side of the sheet, the cross-strand aromatic coupling in **1W-2Y-3L** must be closer to the first turn than are the aromatics in **1L-2Y-3W** to the second turn. The differences in these two peptides suggest that having a cross-strand link far from the turn has less contribution to stability. Moreover, in both these aromatic cross-linked structures, the first hairpin forms much more completely than the second one, and the second one is even more disordered in **1L-2Y-3W**, despite there being an aromatic link between strands 2-3 (see Fig. 1). The variance of structure uniformity in the NMR ensemble and relative T_m values suggest that the overall sequence design acts as the structure and stability driving force and that the aromatic contact is secondary. Here, the ^{D}Pro-Gly sequences stabilize the tight hairpin turns, and the alternation of hydrophobic and hydrophilic groups aids alignment of the residues. Our analyses of the component hairpins gives further evidence to this differentiation.

Consistent with the three-strand data, all the component hairpins have IR spectra suggestive of at least partial β-strand formation (Fig. S5 and S6, SI). For the N-terminal hairpins with no aromatic contacts (**1I-2Y**, **1L-2Y**) the low temperature CD data (Fig. S2, SI) are in line with this, but the C-terminal variant (**2Y-3L**) is less clear. The other two hairpins (**1W-2Y**, **2Y-3W**) have CD dominated by aromatic interaction. Those with Trp-Tyr contacts could potentially be even more stabilized as hairpins, but IR-derived T_m values, reflecting change of β-strand structure, do not seem to differentiate them from similar sequences without Trp-Tyr contacts. Likewise, the β-sheet characteristics are more pronounced in the equilibrium IR spectra for the N-terminal hairpins, as seen from their somewhat sharper maxima occurring at a lower frequency (~1637 cm^{-1}), with the partial exception of **1L-2Y** (Figs. S5 and S6, SI). Our preliminary 1-D NMR data support this as well, with **1W-2Y** and **1I-2Y** having more dispersion in the N-H region than do the other hairpins studied.

The IR transition temperatures also reflect the stability differences between the hairpins constituting strands 1-2 as opposed to the hairpins forming strands 2-3, since the N-terminal variants all have a transition temperature ~20 °C higher than the C-terminal ones (Table S10, SI). The presence or absence of aromatic cross-strand interactions does not seem to impact the T_m significantly, in consideration of the error limits, neither among the N-terminal hairpins, nor among the C-terminal ones. The CD determined T_m values for these hairpins do not provide a clear differentiation, due to their less reliable fits, but for the two with cross-strand aromatic contacts, having more reliable T_m values, that for **1W-2Y** is much higher than for **2Y-3W**. The N-terminal hairpin is consistently seen to be the more stable form. That placement of the aromatics impacted the three-strand sheet stabilities more than for the hairpins may be evidence of the aromatic contact causing a distortion that impacts the

alignment of the third strand with the first two, a problem that would not affect hairpins. One should note that for the previously studied Trpzip2 hairpin peptides and their various mutants, the cross-strand aromatic interaction was a structure driving force and definitely affected the stabilities measured.[6, 17, 43, 45] The major difference between those and the systems studied here is probably the ^{D}Pro-Gly turn sequence, which both stabilizes the turn and prevents complete unfolding.[40, 42, 46]

Comparison of dynamics and relaxation rates. We studied the temperature dependence of relaxation rates and analyzed if there is a correlation between the dynamics of the three-stranded peptides and those of the component hairpins. Table 2 shows selected relaxation times for all variants. They consistently decrease with increasing temperature, as would be expected, but to a different degree. For example, while **1W-2Y** and **1I-2Y** are faster than **1L-2Y** (the outlier) at T_{final} = 10 °C, they are not much different at a higher final temperature of 35 °C. Similarly, while **1W-2Y-3L** and **1I-2Y-3L** are faster than **1L-2Y-3W** at T_{final} = 10 °C, the rates are again quite similar at T_{final} = 35 °C. Furthermore the relative rate pattern is the same in all cases where the three-stranded structure has the slowest rate and its component hairpins are faster with the C-terminal hairpin being in each case the fastest. The temperature dependencies (slopes of the Arrhenius plots) are similar but not identical for each set of fits in Fig. 7, particularly if the outlier points for **1L-2Y** are eliminated.

These Arrhenius plots (Fig. 7 and Fig. S12, SI) are only used to describe qualitative trends, since activation energies for relaxation processes are poorly defined. The three-strand peptides studied here do not fold in an obvious two-state manner. Their broad equilibrium transitions are indicative of a multistate ensemble of structures, whose change in distribution does not allow a quantitative determination of the

equilibrium constants, and consequently prevents detailed analysis of the underlying kinetic steps. Furthermore, the variance in rates for strand and turn segments, although minor, further indicates a non-two-state process.[45]

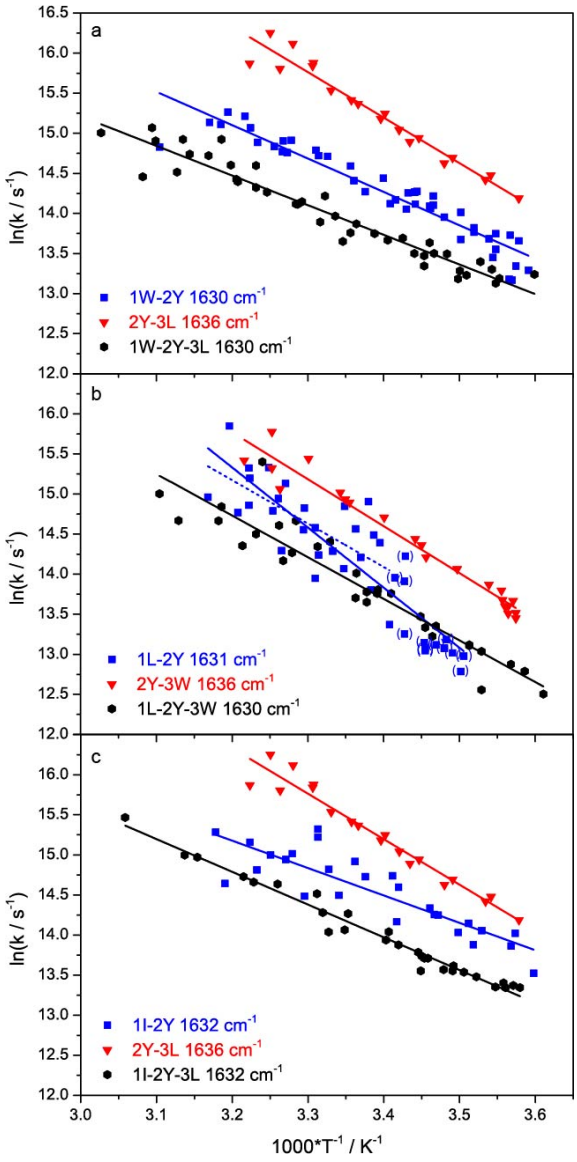

Figure 7: Arrhenius plots (probed at ~ 1630 cm^{-1}) for each three-stranded variant (black) together with its constituent C-terminal (red) and N-terminal hairpins (blue). a) **1W-2Y-3L** (black hexagons) and its constituting hairpins **2Y-3L** (red triangles) and **1W-2Y** (blue squares). b) **1L-2Y-3W** (black hexagons) and its constituting hairpins **2Y-3W** (red triangles) and **1L-2Y** (blue squares). For the N-terminal hairpin **1L-2Y** data points with very low absorbance changes (at low final temperatures below 20°C) were disregarded in the fit for the blue dotted line. c) **1I-2Y-3L** (black hexagons) and its constituting hairpins **2Y-3L** (red triangles) and **1I-2Y** (blue squares).

Variation of dynamics: dependence on both presence and location of aromatic contacts. In contrast to the NMR and equilibrium data, the conformational dynamics, as monitored in the T-jump relaxation processes, are more strongly influenced by the presence as well as the location of an aromatic contact. Fig. 4 illustrates the general trends for the dynamics of the three-stranded β-sheets. The variant without aromatic contact (**1I-2Y-3L**) relaxes fastest as was previously observed for alternate sequences with no aromatic interactions.[11, 35] One factor in the impact of aromatics on rates is displacement of solvent molecules in order facilitate the formation of cross-strand hydrophobic interactions and hydrogen bonds.

The dynamics of the structures having an aromatic contact are slower, and furthermore behave in a site-specific manner, **1L-2Y-3W** being slower than **1W-2Y-3L**. This different effect of the aromatics on dynamics might be explained by the distance between the ^{D}Pro-Gly-turn and the Trp-Tyr cross-strand interaction which is shorter (2 residues) in **1W-2Y-3L** than for **1L-2Y-3W** (3 residues). Similar effects of aromatic contacts on relaxation rates were seen in our previous studies of Trpzip2 based hairpins.[43] There, mutants with two Trp residues substituted with Val (one aromatic contact) had faster dynamics than did Trpzip2 with four Trps (two aromatic contacts). This effect was more evident if the Trp residues farther from the turn were substituted. Thus we also observed a slow-down by aromatic contacts and moreover site-specific dynamics depending on the location of the aromatic contact within the hairpin, namely the closer the aromatic contact is located to the turn, the faster are the dynamics.

Comparing the C-terminal hairpins **2Y-3W** (aromatic contact) and **2Y-3L** (no aromatic contact) (Fig. 5) the relaxation is also slower (at lower temperatures) for the hairpin with a cross-strand aromatic interaction. For the N-terminal hairpins (Fig. 6) we also

see slower dynamics in the presence of aromatic contacts (**1W-2Y** slower than **1I-2Y**), although one hairpin (**1L-2Y)** is an outlier and probably has a sequence-driven effect contributing to its slow rate.

Site-specific dynamics. Comparing the dynamics of the sheets (Fig. 4a) with that of the Xxx-^{D}Pro link, which can sense the turn region (Fig. 4b), the overall trend is the same, although the turn dynamics of **1W-2Y-3L** resemble more those of **1L-2Y-3W** whereas the sheet dynamics of **1W-2Y-3L** are closer to those of **1I-2Y-3L**. A reduction in turn dynamics is correlated to the less-well defined turn that we also observe as a variation in the ensemble of NMR structures (Fig.1), in that **1I-2Y-3L,** without aromatic contact, has no turn variation and the fastest dynamics. The aromatic contact between the sheets may induce structural instability to the turn geometry.

The absorbance changes of the Xxx-^{D}Pro band of the N-terminal hairpins were too small for a reliable analysis. For the C-terminal hairpins, we do not observe a difference in turn vs. sheet dynamics, neither with nor without aromatic contact. This may be a result of the Xxx-^{D}Pro band sensing the turn-to-strand link, not the central turn region, or that the differences are too small to be resolved in our measurements. Selective isotopic labeling might be better suited to probe the turn and the strands individually.

CONCLUSION

Our study of several triple-strand and related hairpin model peptides, designed to have different interactions between the strands, surprisingly showed that the absence of a direct aromatic cross-strand contact did not lead to a significant loss of thermal

stability. The equilibrium properties seem to be dominated by the influence of the ^{D}Pro-Gly turn and general hydrophobic and hydrophilic contacts in the largely conserved sequences and only secondarily affected by the cross-strand aromatic interaction. By contrast, the dynamics, as monitored by the temperature dependencies of the T-jump induced relaxation processes, are more sensitively influenced by the presence and the location of an aromatic interaction. These complexities suggest that the underlying (un)folding mechanism is a multistate process, which is already indicated by the small differences in dynamics observed for the Xxx-^{D}Pro linkage as a site-specific probe. To further evaluate kinetic mechanisms on the basis of individual amino acids, more selective IR probes are needed. Isotope labeling potentially can provide such insight and will be the focus of future study on these systems.

ASSOCIATED CONTENT

Structural data obtained by NMR, CD and FTIR spectra for all variants, tables containing transition temperatures for CD and FTIR, figures comparing the thermal transition of the N- and C-terminal hairpins against the respective three-stranded structures, global fits of the transition temperature for multiple data sets, relaxation times for the N-terminal hairpins and Arrhenius plots of the Xxx-^{D}Pro band of the three stranded variants are provided in a Supporting Information file. This material is available free of charge via the Internet at http://pubs.acs.org.

AUTHOR INFORMATION

Corresponding author:

*E-mail: tak@uic.edu

*E-mail: karin.hauser@uni-konstanz.de

ACKNOWLEDGEMENTS

We gratefully acknowledge financial support by the Deutsche Forschungsgemeinschaft (SFB 969, A2 to K.H.), the Center of Applied Photonics Konstanz (CAP to K.H.), National Science Foundation of China (NSFC 21503087 to H.C.) and Alexander von Humboldt Foundation Research Award (to T.A.K.).

ABBREVIATIONS

COSY, correlated spectroscopy; ^{D}Pro, D-Proline; DTGS, deuterated triglycine sulfate; E_a, activation energy; ECD, electronic circular dichroism; FMOC, Fluorenyl-methyloxycarbonyl; FTIR, Fourier-transform infrared; Gly, Glycine; Ho-YAG, holmium yttrium aluminium garnet; HPLC, high performance liquid chromatography; Leu, Leucine; MALDI, matrix-assisted laser desorption/ionization; MCT, mercury cadmium telluride; NMR, nuclear magnetic resonance; NOESY, nuclear Overhauser effect spectroscopy; Phe, Phenylalanine; QCL, quantum cascade laser; SVD, singular value decomposition; TFA, trifluoroacetate; T-jump, temperature-jump; TOCSY, total correlated spectroscopy; Trp, Tryptophan; Tyr, Tyrosine; UV, ultraviolet; VCD, vibrational circular dichroism

REFERENCES

1. Chiti, F.; Dobson, C.M., Protein Misfolding, Functional Amyloid, and Human Disease. *Annu. Rev. Biochem.* **2006,** *75*, 333-366.
2. McLaurin, J.; Yang, D.S.; Yip, C.M.; Fraser, P.E., Review: Modulating Factors in Amyloid-β Fibril Formation. *J. Struct. Biol.* **2000,** *130*, 259-270.
3. Jiménez, M.A., Design of Monomeric Water-Soluble β-Hairpin and β-Sheet Peptides. In *Protein Design: Methods and Applications*, Köhler, V., Ed. Springer New York: New York, NY, 2014; pp 15-52.
4. Hughes, R.M.; Waters, M.L., Model Systems for β-Hairpins and β-Sheets. *Curr. Opin. Struct. Biol.* **2006,** *16*, 514-524.
5. Setnička, V.; Huang, R.; Thomas, C.L.; Etienne, M.A.; Kubelka, J.; Hammer, R.P.; Keiderling, T.A., IR Study of Cross-Strand Coupling in a β-Hairpin Peptide Using Isotopic Labels. *J. Am. Chem. Soc.* **2005,** *127*, 4992-4993.
6. Hauser, K.; Krejtschi, C.; Huang, R.; Wu, L.; Keiderling, T.A., Site-Specific Relaxation Kinetics of a Tryptophan Zipper Hairpin Peptide Using Temperature-Jump IR Spectroscopy and Isotopic Labeling. *J. Am. Chem. Soc.* **2008,** *130*, 2984-2992.
7. Schenck, H.L.; Gellman, S.H., Use of a Designed Triple-Stranded Antiparallel β-Sheet To Probe β-Sheet Cooperativity in Aqueous Solution. *J. Am. Chem. Soc.* **1998,** *120*, 4869-4870.
8. Koepf, E.K.; Petrassi, H.M.; Sudol, M.; Kelly, J.W., WW: An Isolated Three-Stranded Antiparallel β-Sheet Domain that Unfolds and Refolds Reversibly; Evidence for a Structured Hydrophobic Cluster in Urea and GdnHCl and a Disordered Thermal Unfolded State. *Protein Sci.* **1999,** *8*, 841-853.
9. Griffiths-Jones, S.R.; Searle, M.S., Structure, Folding, and Energetics of Cooperative Interactions between the β-Strands of a de Novo Designed Three-Stranded Antiparallel β-Sheet Peptide. *J. Am. Chem. Soc.* **2000,** *122*, 8350-8356.
10. Nguyen, H.; Jäger, M.; Moretto, A.; Gruebele, M.; Kelly, J.W., Tuning the free-energy landscape of a WW domain by temperature, mutation, and truncation. *Proc. Natl. Acad. Sci. U. S. A.* **2003,** *100*, 3948-3953.
11. Xu, Y.; Purkayastha, P.; Gai, F., Nanosecond Folding Dynamics of a Three-Stranded β-Sheet. *J. Am. Chem. Soc.* **2006,** *128*, 15836-15842.
12. Smith, A.W.; Tokmakoff, A., Amide I Two-Dimensional Infrared Spectroscopy of β-Hairpin Peptides. *J. Chem. Phys.* **2007,** *126*, 045109.
13. Dyer, R.B.; Maness, S.J.; Peterson, E.S.; Franzen, S.; Fesinmeyer, R.M.; Andersen, N.H., The Mechanism of β-Hairpin Formation. *Biochemistry* **2004,** *43*, 11560-11566.
14. Davis, C.M.; Dyer, R.B., WW Domain Folding Complexity Revealed by Infrared Spectroscopy. *Biochemistry* **2014,** *53*, 5476-5484.
15. Du, D.; Zhu, Y.; Huang, C.-Y.; Gai, F., Understanding the Key Factors That Control the Rate of β-Hairpin Folding. *Proc. Natl. Acad. Sci. U. S. A.* **2004,** *101*, 15915-15920.
16. Cochran, A.G.; Skelton, N.J.; Starovasnik, M.A., Tryptophan Zippers: Stable, Monomeric β-Hairpins. *Proc. Natl. Acad. Sci. U. S. A.* **2001,** *98*, 5578-5583.
17. Wu, L.; McElheny, D.; Huang, R.; Keiderling, T.A., Role of Tryptophan−Tryptophan Interactions in Trpzip β-Hairpin Formation, Structure, and Stability. *Biochemistry* **2009,** *48*, 10362-10371.
18. Wu, L.; McElheny, D.; Takekiyo, T.; Keiderling, T.A., Geometry and Efficacy of Cross-Strand Trp/Trp, Trp/Tyr, and Tyr/Tyr Aromatic Interaction in a β-Hairpin Peptide. *Biochemistry* **2010,** *49*, 4705-4714.
19. Roy, A.; Bouř, P.; Keiderling, T.A., TD-DFT Modeling of the Circular Dichroism for a Tryptophan Zipper Peptide With Coupled Aromatic Residues. *Chirality* **2009,** *21*, E163-E171.

20. Tatko, C.D.; Waters, M.L., Selective Aromatic Interactions in β-Hairpin Peptides. *J. Am. Chem. Soc.* **2002,** *124*, 9372-9373.
21. Bieri, O.; Kiefhaber, T., Elementary Steps in Protein Folding. *Biol. Chem.* **1999,** *380*, 923.
22. Callender, R.; Dyer, R.B., Probing Protein Dynamics Using Temperature Jump Relaxation Spectroscopy. *Curr. Opin. Struct. Biol.* **2002,** *12*, 628-633.
23. Robert H. Callender; R. Brian Dyer; Rudolf Gilmanshin; Woodruff, W.H., Fast events in protein folding : The Time Evolution of Primary Processes. *Annu. Rev. Phys. Chem.* **1998,** *49*, 173-202.
24. Haque, T.S.; Gellman, S.H., Insights on β-Hairpin Stability in Aqueous Solution from Peptides with Enforced Type I‘ and Type II‘ β-Turns. *J. Am. Chem. Soc.* **1997,** *119*, 2303-2304.
25. Hwang, T.L.; Shaka, A.J., Water Suppression That Works. Excitation Sculpting Using Arbitrary Wave-Forms and Pulsed-Field Gradients. *J. Magn. Reson., Ser A* **1995,** *112*, 275-279.
26. Delaglio, F.; Grzesiek, S.; Vuister, G.W.; Zhu, G.; Pfeifer, J.; Bax, A., NMRPipe: A multidimensional Spectral Processing System Based on UNIX Pipes. *J. Biomol. NMR* **1995,** *6*, 277-293.
27. Johnson, B.A.; Blevins, R.A., NMR View: A computer Program for the Visualization and Analysis of NMR Data. *J. Biomol. NMR* **1994,** *4*, 603-614.
28. Güntert, P.; Mumenthaler, C.; Wüthrich, K., Torsion Angle Dynamics for NMR Structure Calculation With the New Program Dyana. *J. Mol. Biol.* **1997,** *273*, 283-298.
29. De Guzman, R.N.; Goto, N.K.; Dyson, H.J.; Wright, P.E., Structural Basis for Cooperative Transcription Factor Binding to the CBP Coactivator. *J. Mol. Biol.* **2006,** *355*, 1005-1013.
30. Hornak, V.; Abel, R.; Okur, A.; Strockbine, B.; Roitberg, A.; Simmerling, C., Comparison of Multiple Amber Force Fields and Development of Improved Protein Backbone Parameters. *Proteins: Struct., Funct., Bioinf.* **2006,** *65*, 712-725.
31. Laskowski, R.A.; Rullmann, J.A.C.; MacArthur, M.W.; Kaptein, R.; Thornton, J.M., AQUA and PROCHECK-NMR: Programs for Checking the Quality of Protein Structures Solved by NMR. *J. Biomol. NMR* **1996,** *8*, 477-486.
32. Lakhani, A.; Malon, P.; Keiderling, T.A., Comparison of Vibrational Circular Dichroism Instruments: Development of a New Dispersive VCD. *Applied Spectroscopy* **2009,** *63*, 775-785.
33. Henry, E.R.; Hofrichter, J., Singular Value Decomposition: Application to Analysis of Experimental Data. In *Methods Enzymol.*, Academic Press: 1992; Vol. 210, pp 129-192.
34. Wright Laboratory, The Scripps Research Institute, USA. http://www.scripps.edu/wright/?page_id=17 (accessed December 5, 2017).
35. Popp, A.; Scheerer, D.; Chi, H.; Keiderling, T.A.; Hauser, K., Site-Specific Dynamics of β-Sheet Peptides with DPro–Gly Turns Probed by Laser-Excited Temperature-Jump Infrared Spectroscopy. *Chemphyschem* **2016,** *17*, 1273-1280.
36. Popp, A.; Scheerer, D.; Heck, B.; Hauser, K., Biomolecular Dynamics Studied with IR-Spectroscopy Using Quantum Cascade Lasers Combined With Nanosecond Perturbation Techniques. *Spectrochim. Acta, Part A* **2017,** *181*, 192-199.
37. Wray, W.O.; Aida, T.; Dyer, R.B., Photoacoustic Cavitation and Heat Transfer Effects in the Laser-Induced Temperature Jump in Water. *Appl. Phys. B* **2002,** *74*, 57-66.
38. Wilmot, C.M.; Thornton, J.M., Analysis and Prediction of the Different Types of β-Turn in Proteins. *J. Mol. Biol.* **1988,** *203*, 221-232.

39. Guvench, O.; Brooks, C.L., Tryptophan Side Chain Electrostatic Interactions Determine Edge-to-Face vs Parallel-Displaced Tryptophan Side Chain Geometries in the Designed β-Hairpin “trpzip2”. *J. Am. Chem. Soc.* **2005,** *127*, 4668-4674.
40. Hilario, J.; Kubelka, J.; Keiderling, T.A., Optical Spectroscopic Investigations of Model β-Sheet Hairpins in Aqueous Solution. *J. Am. Chem. Soc.* **2003,** *125*, 7562-7574.
41. Xu, Y.; Oyola, R.; Gai, F., Infrared Study of the Stability and Folding Kinetics of a 15-Residue β-Hairpin. *J. Am. Chem. Soc.* **2003,** *125*, 15388-15394.
42. Gellman, S.H., Minimal Model Systems for β-Sheet Secondary Structure in Proteins. *Curr. Opin. Chem. Biol.* **1998,** *2*, 717-725.
43. Popp, A.; Wu, L.; Keiderling, T.A.; Hauser, K., Effect of Hydrophobic Interactions on the Folding Mechanism of β-Hairpins. *J. Phys. Chem. B* **2014,** *118*, 14234-14242.
44. Du, D.; Tucker, M.J.; Gai, F., Understanding the Mechanism of β-Hairpin Folding via φ-Value Analysis. *Biochemistry* **2006,** *45*, 2668-2678.
45. Krejtschi, C.; Huang, R.; Keiderling, T.A.; Hauser, K., Time-Resolved Temperature-Jump Infrared Spectroscopy of Peptides with Well-Defined Secondary Structure: A Trpzip β-Hairpin Variant as an Example. *Vib. Spectrosc.* **2008,** *48*, 1-7.
46. Awasthi, S.K.; Raghothama, S.; Balaram, P., A Designed β-Hairpin Peptide. *Biochem. Biophys. Res. Commun.* **1995,** *216*, 375-381.

TOC Graphic